Available online at www.sciencedirect.com
ScienceDirect
Journal of Fluorine Chemistry 128 (2007) 448–458
JOURNAL OF FLUORINE CHEMISTRY
www.elsevier.com/locate/fluor

Review

Fluorine insertion reactions into pre-formed metal oxides

Emma E. McCabe, Colin Greaves *

School of Chemistry, University of Birmingham, Edgbaston, Birmingham B15 2TT, United Kingdom

Received 2 October 2006; received in revised form 15 November 2006; accepted 22 November 2006
Available online 25 November 2006

Abstract

Fluorine insertion reactions have been shown to be capable of modifying the physical properties of metal oxide materials, as a result of the structural and electronic consequences of fluorine insertion. This has been applied to copper oxide systems and has led to an enhanced understanding of the requirements for superconductivity, and more recently to other magnetic metal oxide systems where it has been shown to tune the magnetic properties of these materials. This review focuses on some important aspects of research on low temperature fluorine insertion reactions into pre-formed metal oxides, since 1998, and reports some new results.

Keywords: Fluorine insertion; Oxide–fluorides; Transition metal oxide fluorides

Contents

1. Introduction

In 1998, Greaves and Francesconi reviewed the recent research into fluorine insertion reactions in inorganic materials [1]. This review highlighted the advances made in the area of high T_c copper oxide superconductors by low temperature fluorination. Examples include the transformation of semiconducting La_2CuO_4 to p-type superconductor $La_2CuO_4F_\delta$ by oxidative fluorine insertion [2] and the formation of new superconductors such as $Sr_2CuO_2F_{2+\delta}$ by fluorination of the non-superconducting oxide Sr_2CuO_3 [3]. This review illustrated the potential of using soft chemistry routes for the synthesis of novel oxyfluorides rather than standard high temperature solid state reactions. Several low temperature fluorinating agents (discussed in the previous review) can be reacted with a pre-formed metal oxide lattice to give a kinetic or "non-equilibrium" oxide–fluoride product, preserving some structural features of the initial metal oxide. Consequences of insertion into mixed metal oxides can include

(1) reductive anion exchange
   - one O^{2-} anion is substituted by one F^- anion, resulting in reduction of the metal oxide lattice

(2) anion exchange
   - one O^{2-} anion is substituted by two F^- anions, causing neither oxidation or reduction of the metal lattice

* Corresponding author.
E-mail address: c.greaves@bham.ac.uk (C. Greaves).

0022-1139/$ – see front matter © 2006 Elsevier B.V. All rights reserved.
doi:10.1016/j.jfluchem.2006.11.008

(3) oxidative anion insertion
- insertion of F^- into interstitial sites, requiring oxidation of metal oxide lattice

(4) structural rearrangement
- following (1)–(3), the site preferences of oxygen and fluorine may drive a rearrangement of the metal oxide structure.

Since 1998, research in the field of fluorine insertion reactions into copper oxides with applications for high T_c superconductivity has continued and led to an increased understanding of high T_c superconductivity itself and has shed light on the driving forces for structural rearrangements occurring on fluorination. More recently, this knowledge has been applied to non-copper oxide systems where the structural and electronic consequences of fluorine insertion can be used to optimise properties such as magnetism. This has also brought about an increased understanding of structure prediction for oxide–fluorides and the discovery of a new low temperature fluorinating agent. This review focuses on some important aspects of research on low temperature fluorine insertion reactions into pre-formed metal oxides, since 1998, and reports some new results.

2. Fluorine insertion into copper oxides

Initially, the driving force for research into fluorine insertion reactions was to develop new high T_c copper oxide superconducting materials. This meant that both the structural and electronic consequences of fluorination could be exploited. Recent examples of using fluorination to form structural motifs compatible with superconductivity include the fluorination of $Pb_2Sr_2YCu_3O_8$. The structure of this starting oxide is illustrated in Fig. 1(a). Low temperature fluorination with NH_4F results in the formation of PbF_2 (which may provide the driving force for the reaction due to its high lattice energy) and $PbSr_2YCu_3O_6F_4$, illustrated in Fig. 1(b). The fluorination occurs via anion exchange in which O^{2-} anions in the PbO layers are substituted by two F^- anions. A structural rearrangement occurs to provide octahedrally coordinated copper with fluorine in both apical sites and a new CuO_2 plane. The Cu–O framework is oxidised due to the loss of half the Pb^{2+} cations from the structure. Fluorination of this oxide has created two regions which are structurally suitable for superconductivity: a single layer of corner linked CuO_4F_2 octahedra and a double layer of CuO_4F square based pyramids [4].

Fluorination of the T* phase $LaHo_{0.75}Sr_{0.25}CuO_{3.9}$ was found to form two similar T* phases, differing in fluorine content. Fluorination occurred by fluoride insertion into cavities in the rocksalt layers at lower temperatures, whereas at higher temperatures, anion exchange at the apical anion site takes place. The higher fluorine content phase formed has additional anions in the apical site, giving rise to a Jahn–Teller distorted octahedral coordination environment for the copper atoms. Interestingly, due to the presence of anions in the interstitial sites between the rocksalt blocks, the lanthanum, holmium and strontium cations are displaced, leading to a monoclinic symmetry for the material. The lower fluorine content phase formed contained fluorine only in the interstitial sites, which again caused a distortion of the structure, this time involving tilting of the CuO_5 square based pyramids, giving a structure of *Ima*2 symmetry [5].

The Ln_2CuO_4 materials are interesting materials to study in relation to anion insertion due to their differing anion arrangement depending on the size of the lanthanide cation *Ln*. Nd_2CuO_4 adopts a T′ structure and fluorination at very low temperatures leads to oxidative insertion of F^- anions into the structure, forming $Nd_2CuO_4F_x$, in which the copper is oxidised. At slightly higher temperatures (300–400 °C), fluorination occurs via anion exchange, forming the monoclinic phase $Nd_2CuO_3F_2$. As observed for $La_2CuO_{3.6}F_{0.8}$, this oxide–fluoride adopts an intermediate structure between T and T′ structures with an ordered, partial occupation of anion sites between adjacent Nd layers, as well as migration of some anions from the tetrahedrally coordinated interstitial sites in the $Nd_2(O,F)_2$ blocks to octahedral interstices, forming apical vertices of $Cu(O,F)_6$ octahedra. Again, the presence of additional anions in the $Nd_2(O,F)_2$ blocks causes tilting of the $Cu(O,F)_6$ octahedra, in order to reduce anion–anion repulsions [6]. Fluorination at 200 °C of $Nd_2CuO_{3.5}$, an oxygen deficient derivative of the T′ structure, converts the monoclinic oxide into an oxide–fluoride adopting the T′ structure. Fluorination occurs in the fluorite-like Nd_2O_2 blocks, where an F^- anion replaces O^{2-} in a tetrahedral interstitial site. The O^{2-} anion migrates into the vacant anion site in the $CuO_{1.5}\square_{0.5}$ planes forming CuO_2 planes; the migration appears to be electrostatically driven. This process is non-oxidative as oxygen is not lost from the structure. However, additional fluorine can be inserted into the octahedral sites in the $Nd_2(O,F)_2$ blocks forming apical bonds to copper. This oxidation, along with the formation of CuO_2 planes, gives rise to superconductivity in fluorinated $Nd_2CuO_{3.5}$ with a T_c of 6–11 K. At higher temperatures of 300 °C, fluorination occurs via anion exchange, forming the higher fluorine content monoclinic phase $Nd_2Cu(O,F)_5$, also synthesised by the fluorination of Nd_2CuO_4 [7].

These fluorination studies on low dimensional copper oxides revealed the important role of temperature in determining the fluorination route: low reaction temperatures tend to favour fluorine insertion reactions, as in the synthesis of the superconducting fluorinated $Nd_2CuO_{3.5}$ and in the fluorination of $LaHo_{0.75}Sr_{0.25}CuO_{3.9}$; higher reaction temperatures ($T \geq 300$ °C) promote anion exchange, as observed in the synthesis of the monoclinic $Nd_2Cu(O,F)_5$. More significantly, the materials synthesised illustrate the importance of the fluorite like or rocksalt blocks in these layered materials and the different site preferences of oxygen and fluorine. The fluorite like or rocksalt blocks seem to be intrinsic to the fluorination process in the materials studied; fluorination first occurs in these layers with the fluorine anions residing in interstitial sites within these blocks, or in apical positions forming $Cu(O,F)_6$ octahedra, often by anion migration and a structural rearrangement of the starting oxide. This migration is thought to be electrostatically driven and it seems that fluorine anions preferentially occupy the interstitial or apical anion sites, rather

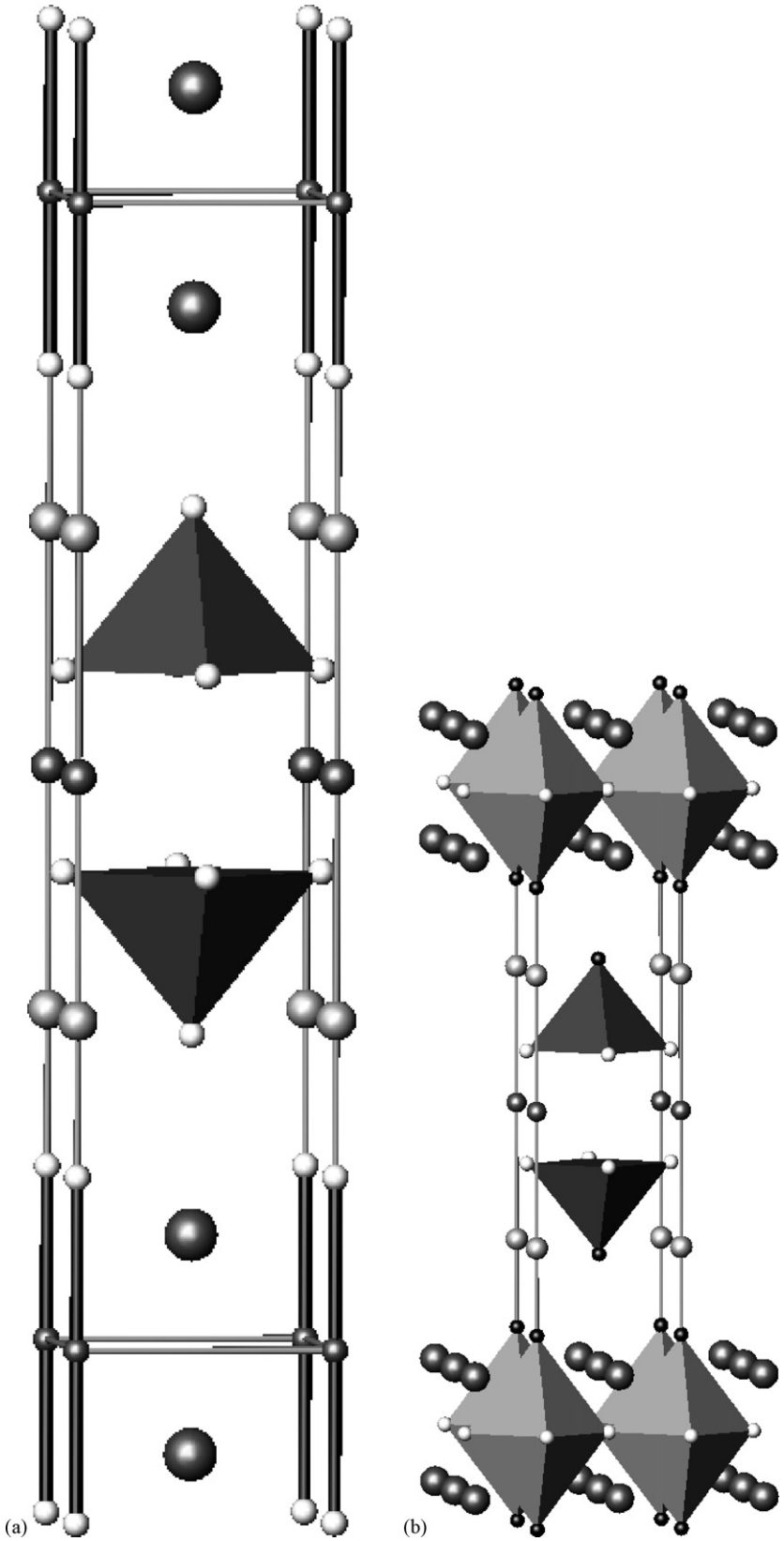

Fig. 1. Structure of (a) $Pb_2Sr_2YCu_3O_8$ and (b) $PbSr_2YCu_3O_6F_4$ showing $Cu(O,F)_5$ and $Cu(O,F)_6$ polyhedra and Sr cations in grey, Pb cations as large dark grey spheres, Y cations as small dark grey sphere, O anions as small white spheres and F anions as small black spheres.

than equatorial sites in the structure, even if these equatorial sites are initially vacant.

Investigations into fluorine insertion into mercury and bismuth containing copper oxides have clearly demonstrated some of the electronic requirements for superconductivity. Superconducting $HgBa_2CuO_{4+\delta}$ (Hg-1201) can be fluorinated to give two phases of differing fluorine contents, the higher fluorine content phase with a slightly reduced T_c (low fluorine content $T_c = 97$ K, high fluorine content $T_c = 96$ K) [8,9]. Interestingly, the amount of additional fluoride anions necessary to obtain the maximum T_c is approximately twice the amount of oxide anions needed, consistent with inserted oxide anions creating twice as many holes as fluoride anions, given the formal valencies of these anions [9]. ^{19}F NMR studies on both fluorinated phases revealed that fluorine is located in a vacant site in the Hg–Hg mesh [8]. Comparison of these phases with the oxygen doped series showed that the additional anions in interstitial sites leads to a contraction of the apical Cu–O bond, but no change in T_c. This suggested that in high pressure studies on superconductors, the increase in T_c was due to contraction of the equatorial Cu–O bond, rather than the apical bond [9] and further ^{19}F NMR studies confirmed the two-dimensional nature of the superconductivity in these materials [10]. The additional anions in the higher fluorine content phase were found to occupy the apical site [11], consistent with the oxygen/fluorine site preferences already observed.

Fluorination of Hg-1223 led to an increase in T_c of 4–138 K [9]. Additional anions were found to occupy two sites in the Hg–Hg mesh. The partial replacement of additional oxygen in this layer by fluorine brought about a contraction in the *ab* plane, leading to shorter equatorial Cu–O bonds and an increase in T_c. This compression of the CuO_2 sheets caused by chemical modification of the structure did not lead to any buckling of the CuO_2 sheets, as is often observed when applying high pressures to these materials [12]. High pressure studies on fluorinated Hg-1223 found this material to have a T_c of 166 ± 1 K, the highest reported at the time of measurement [13].

Surprisingly, fluorination of the Bi-2201 phase occurs via anion exchange, despite the low reaction temperature. Fluoride anions are located between the BiO layers in the interstitial fluorite-type positions. This causes an expansion of this block in the *ab* plane, thereby reducing the size mismatch between the BiO layers and the CuO_2 perovskite blocks and so suppressing the modulations in the structure [14].

Observations from these studies illustrating the relationship between maximum fluorine content and T_c, as well as the observations made concerning the effect of changes in apical and equatorial Cu–O bond lengths on T_c helped enhance the understanding of the electronic requirements for superconductivity. The structural features reported regarding site preferences for oxygen and fluorine are consistent with observations noted from earlier studies [5,7,11].

3. Fluorine insertion into brownmillerite oxides

The brownmillerite structure, of general formula $A_2B_2O_5$, can be described as a layered, perovskite related structure composed of alternating layers of BO_6 octahedra and BO_4 tetrahedra, with the larger A cations in 10 coordinate sites [15], as illustrated in Fig. 2. The first brownmillerite phase to be fluorinated was $LaACuGaO_5$ (A = Sr, Ca). Fluorination was found to occur by anion exchange with one oxygen in the equatorial site in the GaO_4 tetrahedra substituted by two F^- anions, occupying this equatorial site as well as vacant sites in this layer. For both A = Sr and A = Ca, a low fluorine content orthorhombic phase was formed. However, for the larger strontium cation, a higher fluorine content phase could also be synthesised with additional anions randomly distributed throughout the Ga layers [16].

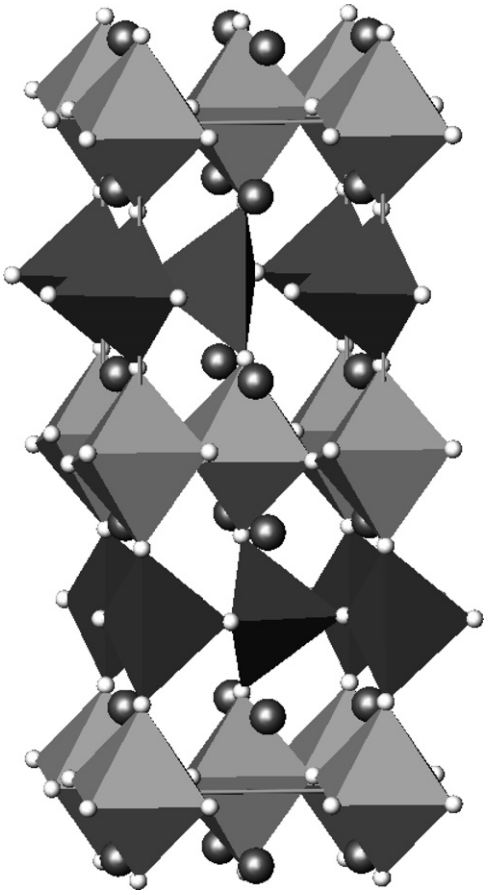

Fig. 2. Structure of brownmillerite $A_2B_2O_5$ with BO_6 octahedra shown in light grey, BO_4 tetrahedra in dark grey, A cations in grey and O anions in white.

However, brownmillerite materials often contain transition metals other than copper with the potential for useful magnetic properties; metals including manganese, iron and cobalt can be accommodated by both octahedral and tetrahedral B cation sites in the brownmillerite structure and the fluorination of several manganese containing phases has been investigated. Fluorination of $Sr_2Mn_2O_5$ results in the formation of the tetragonal phase $SrMn(O,F)_3$ with fluorine filling anion vacancies leading to octahedral coordination for both manganese cations. Measurements of the magnetic properties of this sample revealed a ferromagnetic upturn in susceptibility at 55 K [17]. The authors note that this could result from an amorphous manganese-containing impurity phase in the

sample, but it would be consistent with exchange interactions between d^4 Mn^{3+} and d^3 Mn^{4+} which would be expected to give rise to ferromagnetic coupling.

The fluorination of several phases of general formula $Sr_2MnGaO_{5+\delta}$ with variable oxygen content has also been investigated. The reduced Sr_2MnGaO_5 phase underwent fluorine insertion to give a low fluorine content phase with a similar unit cell to the starting oxide. However, the slightly oxidised $Sr_2MnGaO_{5.5}$ could be fluorinated by anion insertion and reductive anion exchange to form the tetragonal phase $Sr_2MnGaO_{4.78}F_{1.22}$. The fluoride anions are located in the equatorial sites in the GaO layers, forming elongated $Ga(O,F)_6$ octahedra [18]. The apical Ga–O bond remains approximately constant with increasing fluorine content, while the *c* parameter decreases. d^4 Mn^{3+} cations are subject to Jahn–Teller distortions which usually results in an axial elongation of the MnO_6 octahedra. However in this case, the electronically equivalent distortion, involving axial contraction and expansion in the *ab* plane is observed. It is thought that this distortion is electrostatically favoured in order to optimise bonding for the strontium cations [19].

Fluorination of these brownmillerite materials provides one of the few examples of fluoride anions occupying equatorial anion sites. The material $SrMn(O,F)_3$ demonstrates how the oxidative role of fluorine insertion can be exploited to tune the magnetic properties of a material. Ideas relating to the structural and electronic role of fluorination have since been applied to a number of structurally similar non-copper transition metal oxide systems. Work on layered zirconium, titanium and palladium oxides has resulted in an increased understanding of factors enabling structure prediction for the oxide–fluoride product. Research into iron, manganese and ruthenium oxides has added to this knowledge but has also illustrated the potential for the electronic and structural consequences of fluorination to be used to fine tune the magnetic properties of these metal oxide materials.

4. Fluorine insertion into layered zirconium, titanium and palladium oxides

Low temperature fluorination of the Ruddlesden–Popper phase [20] Ba_2ZrO_4 occurs via anion exchange, in which the apical O^{2-} anion is replaced by two F^- anions, additional anions being located in the interstitial sites in the rocksalt layers [21]. Similarly, Sr_2TiO_4 was found to undergo fluorination via anion exchange, with one apical O^{2-} anion substituted by two F^- anions to give an oxide–fluoride product $Sr_2TiO_3F_2$. Again, additional anions occupied interstitial sites in the rocksalt layers. However, an unusual staged arrangement of anions in the interstitial sites was observed, in which alternate layers of interstitial sites within the rocksalt blocks were completely filled, with layers in between being unoccupied [22]. Work on this titanium oxide led to the use of poly(vinylidene fluoride) (PVDF) as a new low temperature fluorinating agent. This reagent tends to work in a non-oxidative fashion via anion exchange. Its advantages over binary fluorides commonly used such as CuF_2 or ZnF_2 are that products are of high quality (no CuO or ZnO byproduct is formed in the reaction) and the organic component is burnt off during the course of the reaction, giving single phase products [23].

Fluorination of the first palladium oxides has recently been reported. $Ba_{2-x}Sr_xPdO_3$ was fluorinated using PVDF at 300–350 °C to form $Ba_{2-x}Sr_xPdO_2F_2$ with the T' structure type. Again, fluorination occurs by anion exchange and a structural rearrangement occurs, similar to that observed on fluorinating Sr_2CuO_3 [2]. On steric grounds, an oxide–fluoride of T structure might have been expected. However, this would impose an octahedral O/F coordination on the Pd^{2+} cations which would have been less favourable on electronic grounds [24]. Unlike the superconducting $Sr_2CuO_2F_{2+\delta}$, these palladium analogues were found not to accommodate excess fluorine in interstitial sites [25].

5. Fluorine insertion into magnetic transition metal oxides

The $n = 2$ manganese Ruddlesden–Popper phase $La_{1.2}Sr_{1.8}Mn_2O_7$, known for exhibiting colossal magnetoresistance (CMR) [26], was fluorinated using CuF_2 to give the oxide–fluoride $La_{1.2}Sr_{1.8}Mn_2O_7F_2$. The fluorination proceeds in an oxidative manner with fluorine being inserted into interstitial sites between the rocksalt layers. This leads to a significant expansion in *c* parameter as the separation between perovskite blocks is increased. The overall structure of the perovskite blocks is preserved, but is noticeably distorted with the apical Mn–O bond directed towards the rocksalt layers being significantly shorter than that in the centre of the perovskite blocks [4].

The fluorination of three iron containing oxides in autoclaves under increased F_2(g) pressure have been reported [27]. The brownmillerite $Sr_2Fe_2O_5$ was fluorinated at 200 °C for 2 days in 2 atm F_2(g) to give two cubic perovskite phases. An anion-deficient Ruddlesden–Popper type phase $Sr_3Fe_2O_6$ was also fluorinated at 120 °C to form the Ruddlesden–Popper oxide–fluoride $Sr_3Fe_2O_6F_{0.87}$. This fluorination proceeds by fluoride insertion oxidising the iron atoms to $Fe^{+3.44}$. This is followed by a structural rearrangement to give the product with fluoride anions in apical sites, as illustrated in Fig. 3. The material shows two-dimensional magnetic ordering with iron atoms within the perovskite bilayers aligned antiferromagnetically. Fluorination of Ba_2InFeO_5 was carried out at 300 °C to give the cubic phase $Ba_2InFeO_5F_{0.68}$, in which oxidative fluorine insertion occurs resulting in a disordered oxygen and fluorine distribution [27]. A further iron oxide, the oxygen deficient perovskite related phase $SrFeO_{3-\delta}$ has also been fluorinated. This fluorination was carried out using PVDF and was found to proceed by reductive anion exchange in which O^{2-} anions are partially replaced by F^- anions, causing reduction of the iron cations and an increase in unit cell size [28].

A second $n = 2$ Ruddlesden–Popper material, $Sr_3Ru_2O_7$, was fluorinated using CuF_2. This reaction resulted in fluorine insertion into the tetrahedral interstitial sites in between the rocksalt layers, while the ruthenium cations were oxidised to

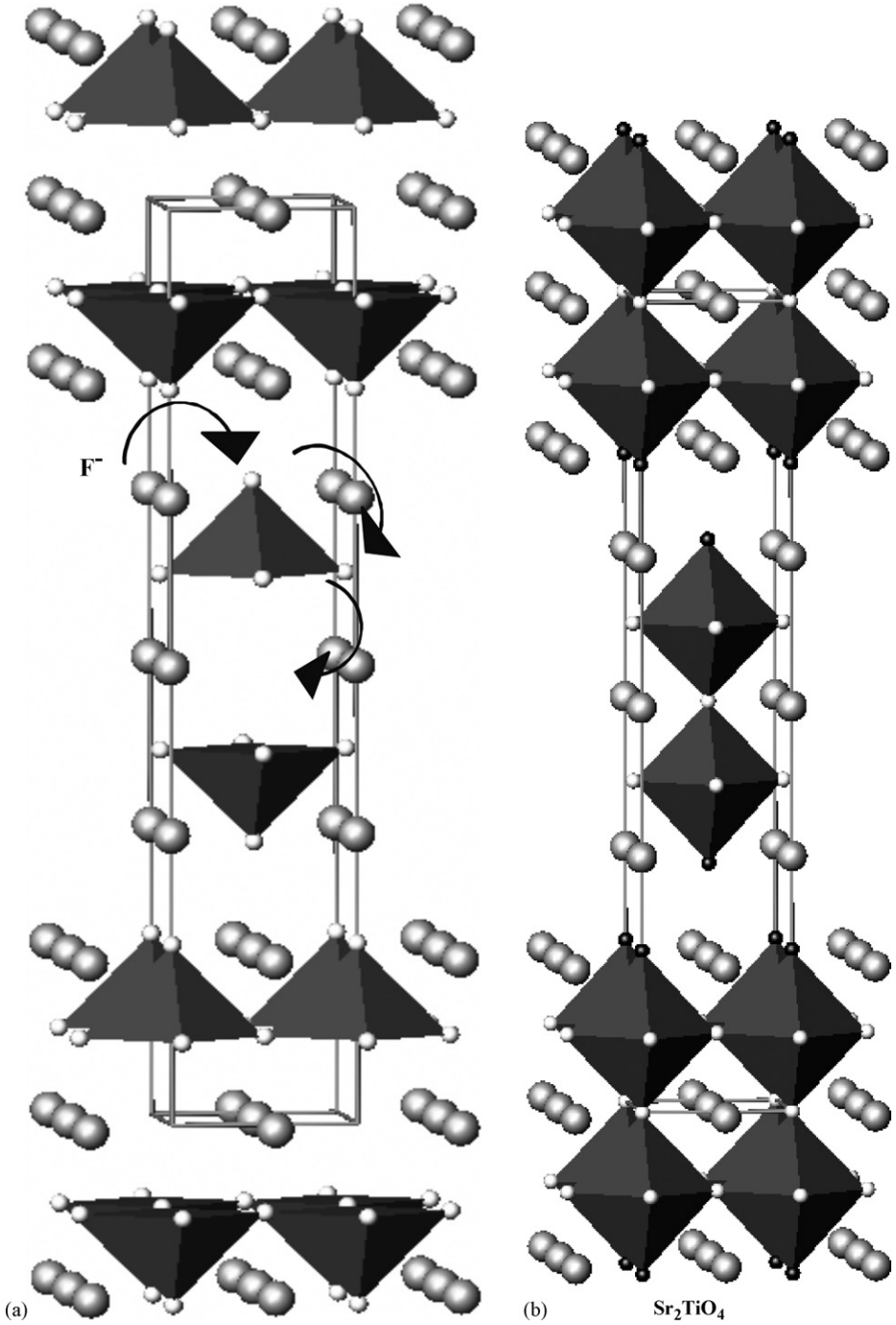

Fig. 3. Fluorination of $Sr_3Fe_2O_6$ to $Sr_3Fe_2O_6F_{0.87}$ showing $Fe(O,F)_5$ and $Fe(O,F)_6$ polyhedra and Sr cations in grey, O anions in white and F anions in black.

give the Ru^{5+} phase $Sr_3Ru_2O_7F_2$. As observed for $La_{1.2}Sr_{1.8}Mn_2O_7F_2$ [4], the external Ru–O apical bond lengths were noticeably shorter than those within the perovskite bilayers. Magnetic measurements of this material revealed an increase in susceptibility on cooling at 185 K, suggesting a ferromagnetic component to the material. However, overall, the material exhibited G type antiferromagnetic ordering which is consistent with Ru t_{2g}–O $2_{p\pi}$–Ru t_{2g} superexchange [29].

Further work on the fluorinated manganese containing Ruddlesden–Popper phases revealed an unusual staged structure with fluoride anions in interstitial sites in alternate rocksalt layers. A similar structure was soon observed for $Sr_2TiO_3F_2$ [22]. This was first observed in the $n = 1$ material $LaSrMnO_4F$ [30]. The oxide precursor $LaSrMnO_4$ was fluorinated using 10% F_2(g)/90% N_2(g) to give a high fluorine content phase $LaSrMnO_4F_{1.7}$, in which the interstitial sites were almost fully occupied by fluoride anions. This oxide–fluoride was then reacted with more of the oxide precursor at 300 °C to give the staged product $LaSrMnO_4F$. In this material, anion sites in the perovskite sheets are thought to be occupied by oxide anions, while the fluoride anions occupy interstitial sites in alternate rocksalt layers [30], as shown in Fig. 4. A staged oxide–fluoride

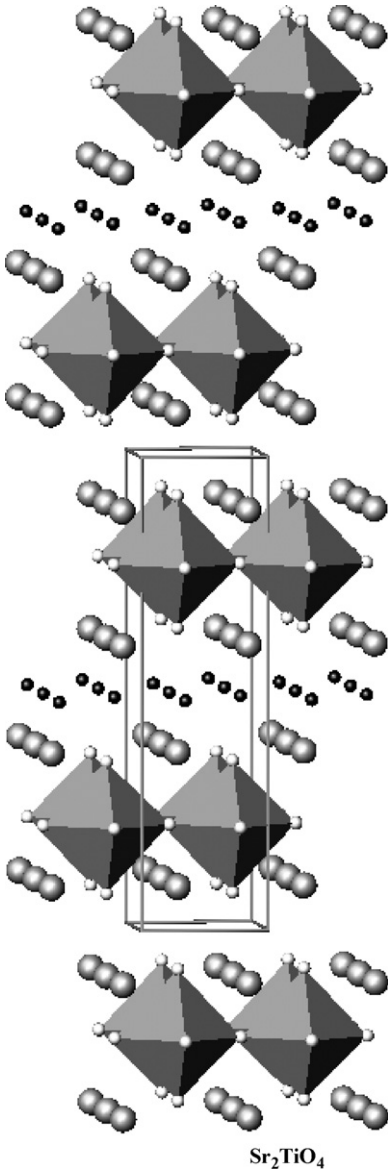

Fig. 4. Structure of $LaSrMnO_4F$ showing MnO_6 polyhedra and La/Sr cations in grey, apical and equatorial anion sites in white and interstitial anion sites in black.

of the $n = 2$ Ruddlesden–Popper phase $La_{1.2}Sr_{1.8}Mn_2O_7$ has also been reported. The fully fluorinated oxide fluoride was synthesised by fluorinating the oxide precursor at 200 °C in 10% F_2(g)/90% N_2(g) to form $La_{1.2}Sr_{1.8}Mn_2O_7F_2$. This was then reacted at 500 °C with the starting oxide to give the staged material $La_{1.2}Sr_{1.8}Mn_2O_7F$. Neither material showed evidence of long range magnetic ordering, but both show unusual distortions of the perovskite blocks. In both materials, the manganese cations are shifted away from the centre of the octahedra, towards the layer of interstitial anions, whilst the oxide anions relax in the opposite direction [31].

6. Recent results on fluorine insertion into iron Ruddlesden–Popper phases

As has already been observed, the layered Ruddlesden–Popper oxide materials readily undergo fluoride insertion reactions. Fluorination occurs in the rocksalt layers initially with fluoride anions occupying interstitial sites in these layers, and also apical anion sites if the reaction has proceeded by anion exchange. Work on the titanium and manganese systems has revealed the possibility of synthesising staged oxide fluoride materials. Two more iron Ruddlesden–Popper oxides have recently been fluorinated and the results of this research are reported here.

6.1. Fluorinated $LaSrFeO_4$

The precursor oxide $LaSrFeO_4$ was synthesised by the sol–gel method using urea. Stoichiometric amounts of $La(NO_3)_3{\cdot}6H_2O$, $Sr(NO_3)_3$ and $Fe(NO_3)_3{\cdot}9H_2O$ were dissolved in 160 cm^3 of water along with 19.22 g of urea. The solution was heated on a hot plate at 80–100 °C with constant stirring as the solvent was evaporated and a brown gel was formed. This was decomposed by heating in air at 300 °C for 3 h, followed by 500 °C for 3 h to form a porous precursor. This was then heated at 1300 °C in air, followed by 1350 °C for 12 h, to form a polycrystalline sample of $LaSrFeO_4$. Structural characterisation of this oxide precursor was carried out using XRPD and the structure was found to be consistent with literature reports [32]. The fluorination of this oxide was carried out at 240 °C for 45 min using 10% F_2/90% N_2 as the fluorinating agent. Thermogravimetric reduction of the oxide–fluoride (using a Rheometric Scientific STA) was used to estimate the fluorine content of the phase. The sample was heated to 1100 °C in 10% H_2 and XRPD analysis showed the material to decompose to LaOF, SrF_2 and Fe. The observed weight loss of 9.83% suggests an initial molecular mass of 390.30 g mol^{-1}. This would be consistent with a composition of $LaSrFeO_3F_3$ for the fluorinated material. Constant wavelength NPD data (λ = 1.59432 Å) for this oxide–fluoride were collected at 2 K on D2B at ILL (Grenoble, France). Magnetic susceptibility was measured by ac excitation (amplitude 5 Oe) and by dc extraction (field of 2500 Oe) using a Quantum Design Physical Properties Measurements System.

A full structural characterisation was carried out using room temperature NPD data. The data were consistent with a tetragonal structure described by *I*4/*mmm* symmetry and there was no evidence of long range magnetic ordering. A structural refinement was carried out using the GSAS suite of programs [33]. It was assumed that additional anions would occupy interstitial sites in between the rocksalt layers and so the structure reported by Soubeyroux et al. [32] was modified in this respect and used as a starting model for the refinement, La_2O_3 was also included in the refinement as a second phase. Background parameters (linear interpolation), histogram scale factors, diffractometer zero points, peak shape and atomic coordinates were refined. The neutron scattering lengths of oxygen and fluorine are almost identical (5.803(4) *fm* and 5.65(1) *fm* for oxygen and fluorine, respectively [34]) and so again no attempt was made to distinguish between the two anions at this stage and anion sites were modelled as occupied by oxygen. The fractional occupancies of the equatorial anion site remained close to full occupancy and so were fixed for the

final refinement cycles. Extremely high thermal parameters were observed for these two anion sites and so the refinement was carried out using anisotropic thermal parameters. Unrealistically high thermal parameters were observed, notably U_{11} and U_{33} for the equatorial site and U_{11} and U_{22} for the apical site. These could reflect some local distortions of the structure. Models were then considered with disordered anion sites: moving the equatorial anions, O/F(eq.), from the 4*c* site to the 8*g* and then 16*n* site significantly improved the model, as did shifting the apical anion, O/F(ap.), from the 4*e* site to the 16*m* site. The displacements of the atoms were then more isotropic and so the thermal parameters were modelled isotropically. The final profile refinements are shown in Fig. 5 and details are given in Table 1. The model is illustrated in Fig. 6 and selected bond lengths are given in Table 2.

The composition $LaSrFeO_3F_3$ suggested by TGA is consistent with the model obtained from analysis of the NPD data, which shows that the structure has equatorial, apical and interstitial anion sites almost fully occupied. This composition suggests that fluoride anions enter the structure through anion exchange in which one O^{2-} anion is substituted by two F^- anions, but also by oxidative insertion, where additional F^- anions enter the structure, oxidising the metal lattice. The anion distribution over these three sites cannot be determined from NPD or XRPD and so bond valence sum (BVS) calculations were carried out [35]. Calculations for the A cation site were inconclusive as this site is occupied by both divalent and trivalent cations and the calculated cation valencies for all anion distributions were between +2 and +3. Similarly for the B cation site, the calculations were inconclusive; this site is likely to be occupied predominantly by Fe^{4+} (as well as a small amount of Fe^{3+}, due to the incomplete filling of the interstitial sites by fluoride anions), which may undergo a Jahn–Teller distortion. Calculations for the anion sites are more informative and are given in Table 3. These results show the most notable anion site preferences are for oxygen to occupy the equatorial anion site and the fluorine to occupy the interstitial anion site, while it seems likely that the apical site is occupied by both oxygen and fluorine. This would be consistent with observations of other fluorinated oxyfluorides reported in the literature where the fluoride anions have a strong preference for the interstitial and apical anion sites. The anion distribution observed here is similar to that described by Slater and Gover [22] for $Sr_2TiO_3F_2$ described above, in which the apical oxygen anion was substituted by two fluoride anions, one of which occupied the apical anion site, the other half occupied the interstitial site in a staged manner. It seems likely that the fluorination of $LaSrFeO_4$ proceeds in a similar manner, but as the Fe^{3+} cation can be oxidised to Fe^{4+}, additional fluorine is able to be inserted into the interstitial sites, leaving

Table 1
Details from refinement of fluorinated $LaSrFeO_4$ in space group *I*4/*mmm* using 2 K NPD data

Atom	*x*	*y*	*z*	Fraction	$U_{iso} \times 100$
La/Sr	0	0	0.3526(2)	0.5/0.5	3.3(1)
Fe	0	0	0	1[a]	2.1(1)
O/F(eq.)	0.045(4)	0.5	0.0365(5)	0.25[a]	6.1(4)
O/F(ap.)	0.080(1)	0.080(1)	0.1160(5)	0.240(4)	3.2(3)
O/F(int.)	0	0.5	0.25	0.911(1)	2.3(1)

a = 3.9099(4) Å, c = 15.660(2) Å; χ^2 = 2.806, R_{wp} = 4.47%, R_p = 3.34%.
[a] Denotes fractional occupancy fixed, see text.

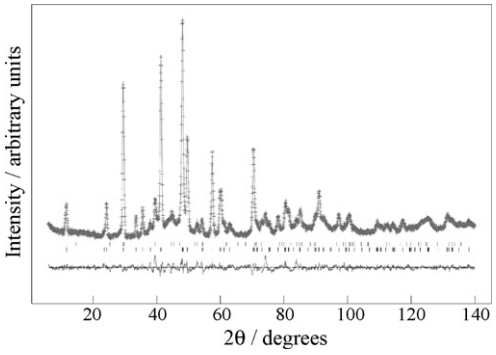

Fig. 5. Observed (+), calculated ((-)) and difference ((-)) profiles from refinement using 2 K NPD data of fluorinated $LaSrFeO_4$ with disordered anion sites, χ^2 = 2.806, R_{wp} = 4.47%, R_p = 3.34%, reflection positions of main phase and of La_2O_3 (10.5(3)% by weight) are marked (|) in black and red, respectively.

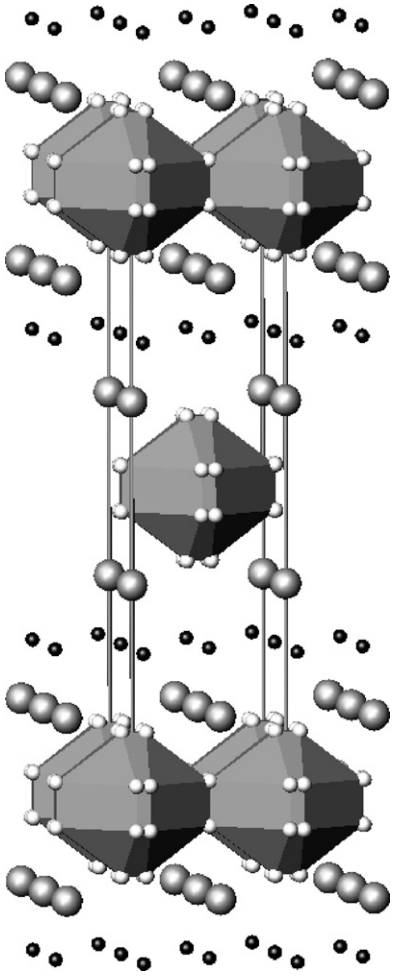

Fig. 6. Structure of fluorinated $LaSrFeO_4$ from 2 K NPD refinement with disordered anion sites, showing distorted FeX_6 polyhedra and La/Sr cations in grey, apical and equatorial anion sites in white and interstitial anion sites in black.

Table 2
Selected bond lengths for fluorinated $LaSrFeO_4$ from 2 K NPD refinement

Bond	Length in Å at 2 K
La/Sr–O/F(eq.)	4 × 2.75(1)
La/Sr–O/F(eq.)	4 × 2.49(1)
La/Sr–O/F(ap.)	8 × 2.843(2)
La/Sr–O/F(ap.)	4 × 2.372(7)
La/Sr–O/F(int.)	4 × 2.531(2)
Fe–O/F(eq.)	16 × 2.045(2)
Fe–O/F(ap.)	8 × 1.870(8)

Table 3
Valencies calculated for anion sites for fluorinated $LaSrFeO_4$ (based on model from 2 K NPD refinement)

Anion X	X(eq.)	X(ap.)	X(int.)
X = O	2.12	1.94	1.41
X = F	1.51	1.37	0.91

them almost fully occupied and the iron oxidised. From the site occupancies determined from NPD refinement, the likely composition of the fluorinated material is $LaSrFeO_{2.96}F_{2.78}$.

The most unusual aspect of the structural model obtained from this study is the distortion of the FeX_6 octahedra; not only are the anions of the apices disordered, but the octahedra are also compressed along the *c* direction, contrary to observations of most A_2BX_4 materials in which, even with no Jahn–Teller distortion, the BX_6 ''octahedra'' are slightly elongated along this direction. This material is thought to contain Fe^{4+} which is a d^4 cation and so susceptible to Jahn–Teller distortions. On CFSE grounds, for d^4 cations, Jahn–Teller distortions comprising expansion in the *ab* plane and axial contraction are energetically equivalent to distortions comprising axial elongation and contraction in the *ab* plane. The latter distortions are more commonly observed in transition metal oxides, but the former has been reported in a manganese oxyfluoride where it was favoured on electrostatic grounds [18]. This may also be the case in this iron oxyfluoride where axial compression of the FeX_6 polyhedra might allow the A cations to form strong interactions with both apical and equatorial anion sites, as well as the interstitial sites. If axial elongation occurred, the A cations might not be able to form such strong interactions with both the equatorial and interstitial anions.

The disordered apices of the FeX_6 polyhedra may be partly due to the joint occupation of the apical anion site by oxygen and fluorine, but might also reflect some local distortion of the perovskite sheets. It is unlikely that this would occur to optimise bonding for the B site which is occupied by the small Fe^{4+} cation, as octahedral tilting will tend to increase B–X bond lengths. Distortions may occur in order to reduce anion–anion repulsions: with additional anions in between the rocksalt layers, the apical anions may shift away from their special positions to increase the anion–anion separation. In order to maintain an appropriate geometry for the B cation site, the equatorial anions will then also move off their ideal, high symmetry positions.

Magnetic measurement performed on the oxide–fluoride show an increase in susceptibility on cooling and the field cooled and zero-field cooled datasets begin to diverge below 180 K. This is consistent with the NPD data collected at low temperature which gave no evidence of long range magnetic ordering. The plot of inverse susceptibility versus temperature is nonlinear below 150 K and so only the high temperature range was used to calculate the Curie–Weiss paramagnetic moment. From the FC data, the moment was calculated as $3.15\mu_B$. This is significantly lower than would be expected for a d^4 Fe^{4+} cation (theoretical spin-only moment of $4.899\mu_B$). The low moment observed probably reflects the fact that the material does not behave as an ideal paramagnet, and that there may be some antiferromagnetic interactions between adjacent iron cations.

6.2. *Fluorinated $La_2SrFe_2O_7$*

Fluorination of the $n = 2$ Ruddlesden–Popper phase $La_2SrFe_2O_7$ has also been investigated. A polycrystalline sample of $La_2SrFe_2O_7$ was synthesised by the solid state reaction of stoichiometric quantities of high purity La_2O_3, $SrCO_3$ and Fe_2O_3 (Aldrich, >99%). The reagents were intimately ground together and heated at 1350 °C for 12 h followed by 1375 °C for 24 h with

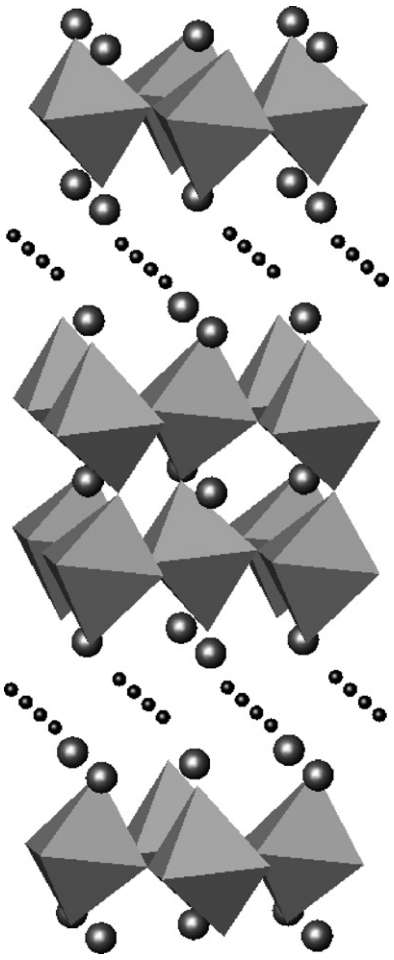

Fig. 7. Predicted structure of $La_2SrFe_2O_7F_2$ showing tilting of FeX_6 polyhedra and La/Sr cations in grey, apical and equatorial anion sites in white and interstitial anion sites in black.

intermittent grinding. Structural characterisation of this oxide precursor was carried out using XRPD and the structure was found to be consistent with literature reports [36]. This oxide was fluorinated at 290 °C in flowing 10% F_2(g) for 6 h, following by leaving the sample in static 10% F_2(g) at 290 °C for 12 h to form the fully fluorinated oxide $La_2SrFe_2O_7F_2$. This oxide–fluoride was then reacted with the oxide precursor (the oxide–fluoride slightly in excess) to give the staged, partially fluorinated phase $La_2SrFe_2O_7F$. Again, thermogravimetric reduction of the oxide–fluoride phases (using a Rheometric Scientific STA) was used to estimate the fluorine content of the two samples. The samples were heated to 1100 °C in 10% H_2 and XRPD analysis showed the materials to decompose. The observed mass losses were consistent with compositions of $La_2SrFe_2O_7F_2$ and $La_2SrFe_2O_7F$ for the two phases. Room temperature XRPD data were collected over a period of 10 h at room temperature on a Siemens D5000 diffractometer (operating in transmission mode with a monochromated Cu Kα1 radiation source, a step size of 0.0204° and a position sensitive detector).

As observed for the manganese analogue $La_{1.2}Sr_{1.8}Mn_2O_7$, a fully fluorinated oxide fluoride material can be synthesised, as well as a partially fluorinated phase. However, unlike the manganese analogues, both the fully fluorinated material $La_2SrFe_2O_7F_2$, as well as the partially fluorinated phase $La_2SrFe_2O_7F$, adopt distorted structures with tilting of the FeX_6 octahedra in the perovskite layers. An example of such a structure proposed for $La_2SrFe_2O_7F_2$ is illustrated in Fig. 7. Preliminary studies suggest that the partially fluorinated phase $La_2SrFe_2O_7F$ adopts the novel staged structure with additional anions located in interstitial sites in alternate rocksalt layers. Detailed structural investigations, as well as measurements of the magnetic properties of these materials, are currently underway.

7. Concluding remarks

Fluorine insertion reactions were used initially to develop new high T_c superconducting copper oxide systems [2] and have since led to an increased understanding of the structural and electronic requirements for superconductivity [10]. Recent research has shown how the electronic and structural consequences of fluorine insertion can be exploited to modify the magnetic properties of materials [29]. Fluorination studies over the last 8 years have highlighted some of the structural features of fluorination reactions, including the important role of the rocksalt/fluorite like blocks between the perovskite-related layers, as well as the different site preferences of oxide and fluoride anions. A novel structure type, resulting from staged anion insertion, has also been reported for a number of materials [22,30,31]. This presents a further possibility for controlling the oxidative effect of fluorination, as well as the structural consequences; these have yet to be investigated for the two phases resulting from the fluorination of $La_2SrFe_2O_7$.

Acknowledgments

We are grateful to Dr. L.J. Gillie, Dr. R.K. Li, Dr. A. Kirbyshire and Miss E.C. Sullivan for help with fluorination reactions and the fluorination apparatus. We would also like to thank Dr. E. Suard and Dr. R. Smith for assistance collecting NPD data. We are grateful to EPSRC and University of Birmingham for funding.

References

[1] C. Greaves, M.G. Francesconi, Curr. Opin. Solid State Mater. Sci. 3 (1998) 132–136.
[2] B. Chevalier, A. Tressaud, B. Lepine, K. Amine, J.M. Dance, L. Lozano, E. Hickey, J. Etourneau, Phys. C 167 (1990) 97–101.
[3] M. Al-Mamouri, P.P. Edwards, C. Greaves, M. Slaski, Nature 364 (1994) 382–384.
[4] C. Greaves, J.L. Kissick, M.G. Francesconi, L.D. Aikens, L.J. Gillie, J. Mater. Chem. 9 (1999) 111–116.
[5] J. Hadermann, A.M. Abakumov, O.I. Lebedev, G. van Tenderloo, M.G. Rozova, R.V. Shpanchenko, B.P. Pavljuk, E.M. Kopnin, E.V. Antipov, J. Solid State Chem. 147 (1999) 647–656.
[6] J. Hadermann, G. van Tenderloo, A.M. Abakumov, M.G. Rozova, E.V. Antipov, J. Solid State Chem. 157 (2001) 56–61.
[7] G. Corbel, J.P. Attfield, J. Hadermann, A.M. Abakumov, A.M. Alekseeva, M.G. Rozova, E.V. Antipov, Chem. Mater. 15 (2003) 189–195.
[8] E.V. Antipov, A.M. Abakumov, K.A. Lokshin, D.A. Pavlov, M.G. Rozova, S.N. Putilin, A.M. Balagurov, D.V. Sheptyakov, Phys. C 341–348 (2000) 579–580.
[9] S.N. Putilin, E.V. Antipov, A.M. Abakumov, M.G. Rozova, K.A. Lokshin, D.A. Pavlov, A.M. Balagurov, D.V. Sheptyakov, M. Marezio, Phys. C 338 (2000) 52–59.
[10] E.N. Morozova, A.A. Gippius, E.V. Antipov, K. Luders, W. Hoffmann, Phys. B 284–288 (2000) 869–870.
[11] A.A. Gippius, E.V. Antipov, O. Klein, K. Luders, Phys. C 284–288 (2000) 935–936.
[12] K.A. Lokshin, D.A. Pavlov, S.N. Putilin, E.V. Antipov, D.V. Sheptyakov, A.M. Balagurov, Phys. Rev. B 63 (2001), 064511(1-5).
[13] M. Monteverde, C. Acha, M. Nunez-Requeiro, D.A. Pavlov, K.A. Lokshin, S.N. Putilin, E.V. Antipov, Europhys. Lett. 72 (2005) 458–464.
[14] J. Hadermann, N.R. Khasanova, G. van Tenderloo, A.M. Abakumov, M.G. Rozova, A.M. Alekseeva, E.V. Antipov, J. Solid State Chem. 156 (2001) 445–451.
[15] E. Bertaut, P. Blum, A. Sagnieres, Acta Cryst. 12 (1959) 149–159.
[16] J. Hadermann, G. van Tendeloo, A.M. Abakumov, B.P. Pavlyuk, M. Rozova, E.V. Antipov, Int. J. Inorg. Mater. 2 (2000) 493–502.
[17] M.V. Lobanov, A.M. Abakumov, A.V. Sidorova, M.G. Rozova, O.G. D'yachenko, E.V. Antipov, J. Hadermann, G. van Tendeloo, Solid State Sci. 4 (2002) 19–22.
[18] A.M. Alekseeva, A.M. Abakumov, M.G. Rozova, E.V. Antipov, J. Hadermann, J. Solid State Chem. 177 (2004) 731–738.
[19] E.V. Antipov, A.M. Abakumov, A.M. Alekseeva, M.G. Rozova, J. Hadermann, O.I. Lebedev, G. van Tendeloo, Phys. Stat. Sol. (a) 201 (2004) 1403–1409.
[20] S.N. Ruddlesden, P. Popper, Acta Cryst. 10 (1957) 538–540.
[21] P.R. Slater, R.K.B. Gover, J. Mater. Chem. 11 (2001) 2035–2038.
[22] P.R. Slater, R.K.B. Gover, J. Mater. Chem. 12 (2002) 291–294.
[23] P.R. Slater, J. Fluorine Chem. 117 (2002) 43–45.
[24] T. Baikie, E.L. Dixon, J.F. Rooms, N.A. Young, M.G. Francesconi, Chem. Commun. (2003) 1580–1581.
[25] T. Baikie, M.S. Islam, M.G. Francesconi, J. Mater. Chem. 15 (2005) 119–123.
[26] Y. Moritomo, A. Asamitsu, H. Kuwahara, Y. Tokura, Nature 380 (1996) 141–144.
[27] G.S. Case, A.L. Hector, W. Levason, R.L. Needs, M.F. Thomas, M.T. Weller, J. Mater. Chem. 9 (1999) 2821–2827.
[28] F.J. Berry, X. Ren, R. Heap, P. Slater, M.F. Thomas, Solid State Commun. 134 (2005) 621–624.
[29] R.K. Li, C. Greaves, Phys. Rev. B 62 (2000) 3811–3815.

[30] L.D. Aikens, R.K. Li, C. Greaves, Chem. Commun. (2000) 2129–2130.
[31] L.D. Aikens, L.J. Gillie, R.K. Li, C. Greaves, J. Mater. Chem. 12 (2002) 264–267.
[32] J.L. Soubeyroux, P. Courbin, L. Fournes, D. Fruchart, G.L. Flem, J. Solid State Chem. 31 (1980) 313–320.
[33] A.C. Larson, R.B.v. Dreele, GSAS, 1987.
[34] Neutron News 3 (1992) 29–37.
[35] I.D. Brown, D. Altermatt, Acta Cryst. B41 (1985) 244–247.
[36] I.B. Sharma, D. Singh, S.K. Magotra, J. Alloys Compd. 269 (1998) 13–16.